M. Pugliatti, A. Rizza, F. Piccolo, V. Franzese, C. Bottiglieri, C. Giordano, F. Ferrari, F. Topputo
The Milani Mission: Overview and Architecture of the Optical-Based GNC System
in: AIAA Scitech 2022 Forum, AIAA, 2022, ISBN: 9781624106316, p. 1-20, AIAA 2022-2381
[AIAA Scitech 2022 Forum, San Diego, CA, USA & Virtual Conference, 3-7 Jan. 2022]
doi:10.2514/6.2022-2381

The Milani mission: overview and architecture of the optical-based GNC system.

M. Pugliatti *, A. Rizza *, F. Piccolo *, V. Franzese †, C. Bottiglieri ‡, C. Giordano †, F. Ferrari§, F. Topputo ¶
Department of Aerospace Science and Technology, Politecnico di Milano, Via La Masa 34, 20156, Milan, Italy.

Milani is a 6U CubeSat that will be part of the Hera mission around the Didymos binary system. Its objectives are both scientific and technological: to study and characterize the Didymos environment, and to demonstrate the use of CubeSat technologies for interplanetary missions. The latter includes the usage of autonomous navigation algorithms in a close-proximity environment. The purpose of this work is twofold. First, to provide an updated overview of the Milani mission. Second, for the first time, to illustrate the architecture and some preliminary results of the semi-autonomous optical-based GNC system.

I. Introduction

Small bodies in the Solar System represent the current frontier in space exploration. Various missions such as Rosetta [1], Hayabusa 1 [2] and 2 [3], and Osiris-Rex [4] have been launched towards these targets, while others are planned for the future [5, 6]. When arrived in the proximity of a small body, deep-space CubeSats offer the advantage of diversifying and complementing large spacecraft missions [7]. Indeed, they can be exploited as opportunistic payloads to be deployed in situ, once the main spacecraft has reached its target. An example is given by the AIDA (Asteroid Impact and Deflection Assessment) collaboration between NASA and ESA to study and characterize an impact with the Didymos asteroid system [8]. As part of this collaboration, NASA launched the DART (Double Asteroid Redirection Test) kinetic impactor spacecraft [9], whose impact with the secondary asteroid of Didymos will be observed and characterized by LICIACube in autumn 2022 [10]. As part of this cooperation, ESA will launch in October 2024 the Hera mission [6] together with two deep-space CubeSats, namely Juventas [11] and Milani [12–14], to study and characterize the system. Shortly after Hera's arrival in January 2027, an early characterization phase between 20 and 30 km distance will aim at determining the shape and the gravity field of the bodies. A detailed characterization phase will follow from about 10-20 km distance. During this phase the two CubeSats will be released from the Hera mothercraft, enhancing the scientific return of the mission. Juventas will be equipped with a monostatic low-frequency radar as well as accelerometers, while Milani will carry the ASPECT [15] visual and near-IR imaging spectrometer and VISTA thermogravimeter [16] to characterize the dust environment around the asteroid.

Autonomous Optical Navigation (OpNav) is an enabling technology for present and future exploration missions. Such technique exploits Image Processing (IP) methods to extract a set of optical observables which is used to generate a state estimate with associated uncertainties. Such estimate is often obtained through filtering, which combines information from the dynamics with an observation model to achieve much higher accuracy than from the application of the IP alone. Since images can be inexpensively generated on-board with low-cost and low-mass sensors, OpNav is experiencing a growing interest for on-board applications. This is particularly relevant for CubeSat missions, which are often tightly constrained in terms of mass and power. In the case of proximity to small-bodies, OpNav can be exploited to reduce operational costs by allowing autonomous operations and unlocking the capabilities to perform critical operations. By linking OpNav capabilities with Guidance and Control algorithms, autonomous GNC systems can be foreseen in the near future in self-exploring missions with reduced or complete absence of humans-in-the-loop.

In this work, for the first time, we present the key characteristics of the OpNav based GNC system of the Milani mission together with an updated overview on the status of the mission. The rest of the paper is organized as follows. In Section II a generic overview of the Milani mission is provided. In Section III the GNC system of Milani is illustrated in detail. This is done starting from the IP in Section III.A, followed by the navigation in Section III.B and guidance and control in Section III.C. To conclude the GNC of Milani a brief overview is given about the preliminary design of the

*PhD student, Department of Aerospace Science and Technology, Politecnico di Milano, mattia.pugliatti@polimi.it
†PostDoc fellow, Department of Aerospace Science and Technology, Politecnico di Milano
‡Research assistant, Department of Aerospace Science and Technology, Politecnico di Milano
§External collaborator, University of Bern, Physics Institute, Gesellschaftsstrasse 6, 3012 Bern, Switzerland
¶Full professor, Department of Aerospace Science and Technology, Politecnico di Milano

autonomous OpNav experiment in Section III.D. In Section IV the results of some analysis generated with the described GNC system are illustrated. Finally, in Section V the main findings presented here are discussed together with some remarks for future works.

II. Mission overview

Milani is a 6U CubeSat that will be launched as a piggyback of the Hera spacecraft towards the Didymos binary system in 2024. After arriving at the system in 2027, Milani will be released from Hera and will focus on its scientific objectives, related to the characterization of Didymos' asteroids and their environment. The primary and secondary bodies of the system are called Didymos and Dimorphos (for simplicity, also referred to as D1 and D2, respectively). D1 is estimated to be an irregular-spherical-like body with a diameter of 780 m while D2 is modeled as a triaxial ellipsoid with a major axis of 170 m. Milani's objectives are twofold: both scientific and technological. From a scientific point of view the main objectives are to:

- **Study and characterize the Didymos binary system.** This includes support to Hera for the determination of the global properties of the system, characterization of the surface of both bodies, evaluation of space weathering phenomena, and characterization of surface properties near the crater.
- **Support the gravity field estimation.** This is achieved passively by the range and range-rate measurements exchanged between Milani and Hera via the Inter Satellite Link (ISL) network during the entire mission.
- **Characterization of the dust environment.** This includes the detection of inorganic materials, volatiles, and light organics within the asteroid environment and in deep-space.

The scientific objectives are achieved by a global mapping of the two asteroids, high-resolution images of the crater on D2, surface micro-structure characterization of both bodies done with the ASPECT payload [15], while radio-science and dust environment experiments are performed respectively with the ISL and the VISTA [16]. From a scientific point of view, D2 and observations of its crater are the main focus of the Milani mission. From a technological point of view, Milani main objectives are to:

- **Provide ISL communication with Hera.** This translates into the demonstration of the operability of a inter-satellite local network in deep-space.
- **Demonstrate the use of CubeSat technologies in deep-space.** This includes the capability to provide relative positioning to Hera, to measure the effects of the asteroid environment on key hardware, and to validate autonomous navigation algorithms. The latter is the main focus of the work presented here.

To accomplish both sets of objectives, Milani is designed as a 6U CubeSat with orbital and attitude control capabilities and deployable solar arrays. In addition to ASPECT, VISTA, and the ISL antennas, Milani is currently designed to host a NavCam (21×16 deg FOV, with a 2048×1536 pixels wide sensor mounted co-axially with respect to ASPECT), a lidar, sun-sensors, a star-tracker, and an IMU.

Milani's mission phases are schematized in Figure 1 and Figure 2. Their detailed descriptions are beyond the scope of this work, which focuses in its analysis on the two main phases of the mission: the Far Range Phase (FRP) and Close Range Phase (CRP).

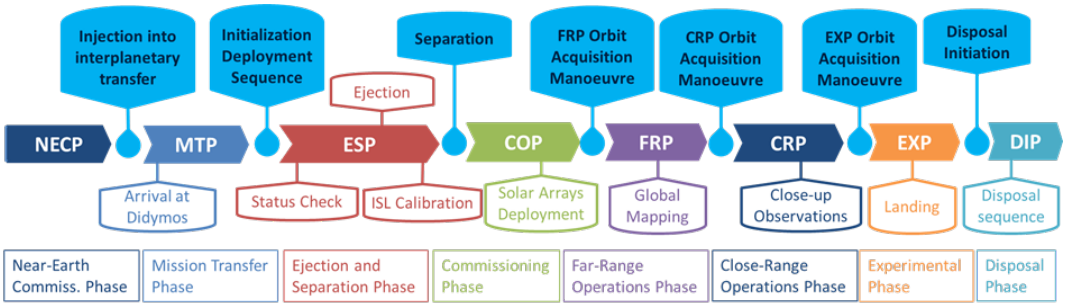

Fig. 1 Phases of the Milani mission.

The trajectory design process in the Didymos system is strongly influenced by the effect of gravitational and Solar Radiation Pressure (SRP) perturbations and by the use of a passive payload (ASPECT) [12, 13]. Because of this, Milani's proximity trajectories have been designed to hover above the Didymos system during FRP and CRP exploiting hyperbolic arcs, as illustrated in Figure 3.

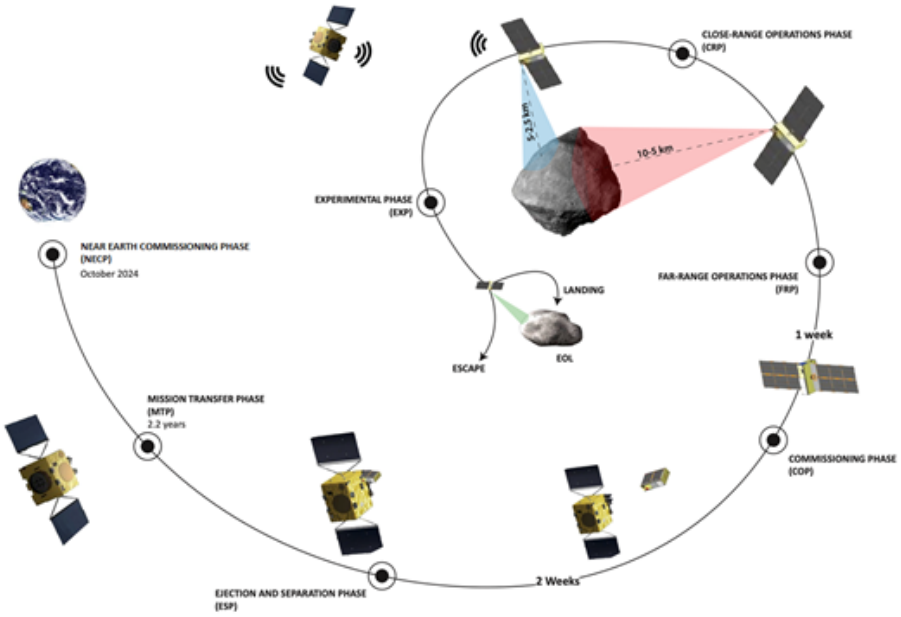

Fig. 2 Schematics of the phases of the Milani mission.

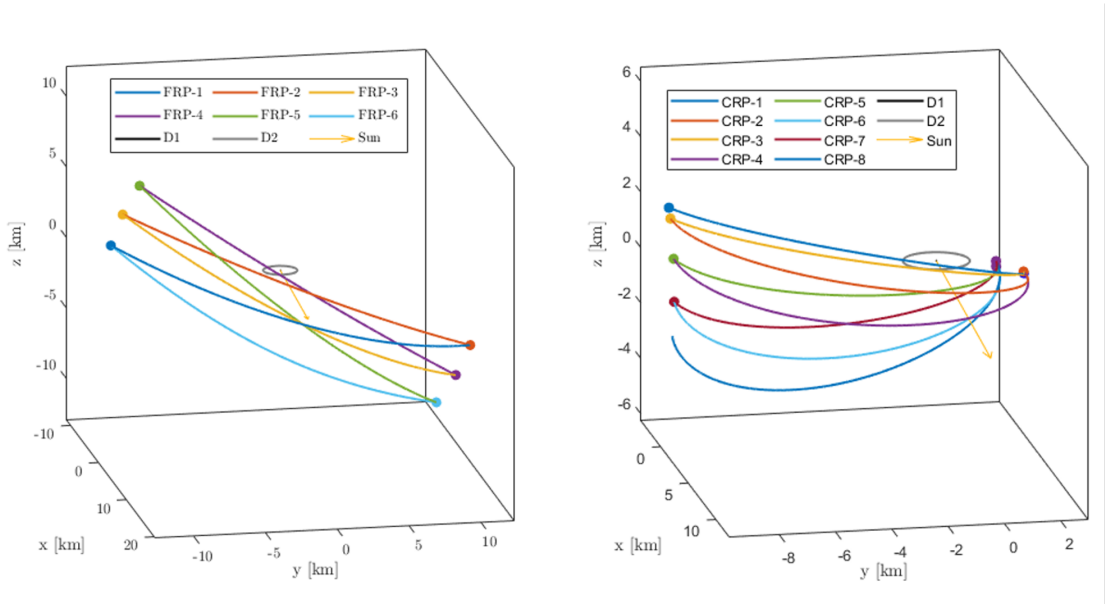

Fig. 3 Arcs of the FRP (left) and CRP (right) phases of the Milani mission seen in an inertial fixed reference frame w.r.t. the Sun (Orange arrow).

The FRP and CRP last roughly 21 and 28 days respectively. As it is possible to see in Figure 3, the FRP exhibits symmetrical arcs that develop within 8-14 km from D1 while the CRP exhibits asymmetrical arcs within 2-11 km. To conclude the mission after the main scientific objectives are achieved, the CRP will be followed by an Experimental Phase (EXP) which will climax in a landing attempt on D2. In Figure 4 it is possible to see the values of the phase angle, range, and apparent size of D1 and D2 during the Commissioning Phase (COP), FRP, CRP, and EXP phases of the mission.

Various works in the literature are sprouting that illustrate different aspects of the Milani missions. The most relevant ones are briefly listed here for the interested reader to provide context for what is presented and what is omitted in

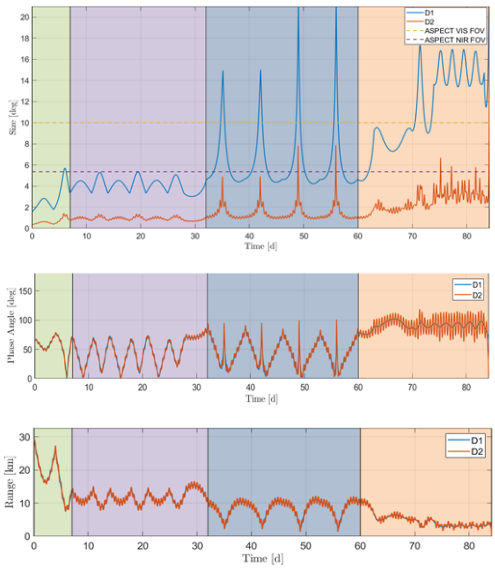

Fig. 4 From bottom to top: Milani's range, and phase angles w.r.t. D1 and D2, and apparent size of D1 and D2. The colors represent the COP, FRP, CRP, and EXP phases illustrated in Figure 1 and Figure 2.

this work. The process of designing close-proximity operations in a binary asteroid system is discussed at length in [13] while the preliminary mission analysis and GNC design of Milani which constituted the proposal and phase 0 of the mission are illustrated in [12]. A detailed description of the IP can be found in [17, 18]. In [14] the important relationship between the trajectory design and orbit determination processes is shown. The interested reader is also directed to [15, 16] for details about VISTA and ASPECT, respectively.

Milani consortium is composed of entities and institutions from Italy, Czech Republic, and Finland. Consortium Prime is Tyvak International, responsible for the whole program management and platform design, development, integration, testing, and final delivery to the customer. Politecnico di Torino is dealing with requirements definition, thermal analysis, radiation analysis, and debris analysis. Politecnico di Milano is responsible for Mission Analysis and GNC. Altec will support the Ground Segment architecture and interfaces definition. Centro Italiano per la Ricerca Aerospaziale (CIRA) will be responsible for the execution of the vehicle environmental campaign. HULD will contribute to developing the mission-specific software. VTT is the main payload (ASPECT, spectral imager) provider, and is supported by the following entities dealing with ASPECT-related development: University of Helsinki (ASPECT calibration), Reaktor Space Lab (ASPECT Data Processing Unit development), Institute of Geology – the Czech Republic Academy of Science (ASPECT scientific algorithms requirements and testing), Brno University of Technology (ASPECT scientific algorithms development). INAF-IAPS is the secondary Payload (VISTA, dust detector) provider.

Throughout its design phase, the Milani mission has been characterized by a fast development cycle. Phase 0 took place during proposal preparation in Spring 2020. The Milani team successfully passed the Preliminary Design Review (PDR) in summer 2021 and is currently in phase C until the Critical Design Review (CDR), scheduled in spring 2022.

III. GNC

Milani GNC is designed with semi-autonomous capabilities enabled by innovative image processing and autonomous navigation components paired with traditional guidance and control logic. The design philosophy of the GNC has been driven by the following goal: to be able to generate a primary pointing for the ADCS in a robust, simple, and precise way across the different mission scenarios. To do so, Milani's GNC uses a series of strategies which at the highest level of autonomy rely on visual-based navigation algorithms. The AOCS (considered here as the union of GNC and ADCS) is then responsible for the full 6D orbital-attitude navigation, guidance, and control of the CubeSat. Since the Milani GNC system generates autonomously an on-board primary pointing profile as output, and since it does not have on-board autonomous guidance and control, the system is defined as semi-autonomous. The overall architecture of the GNC is illustrated in Figure 5.

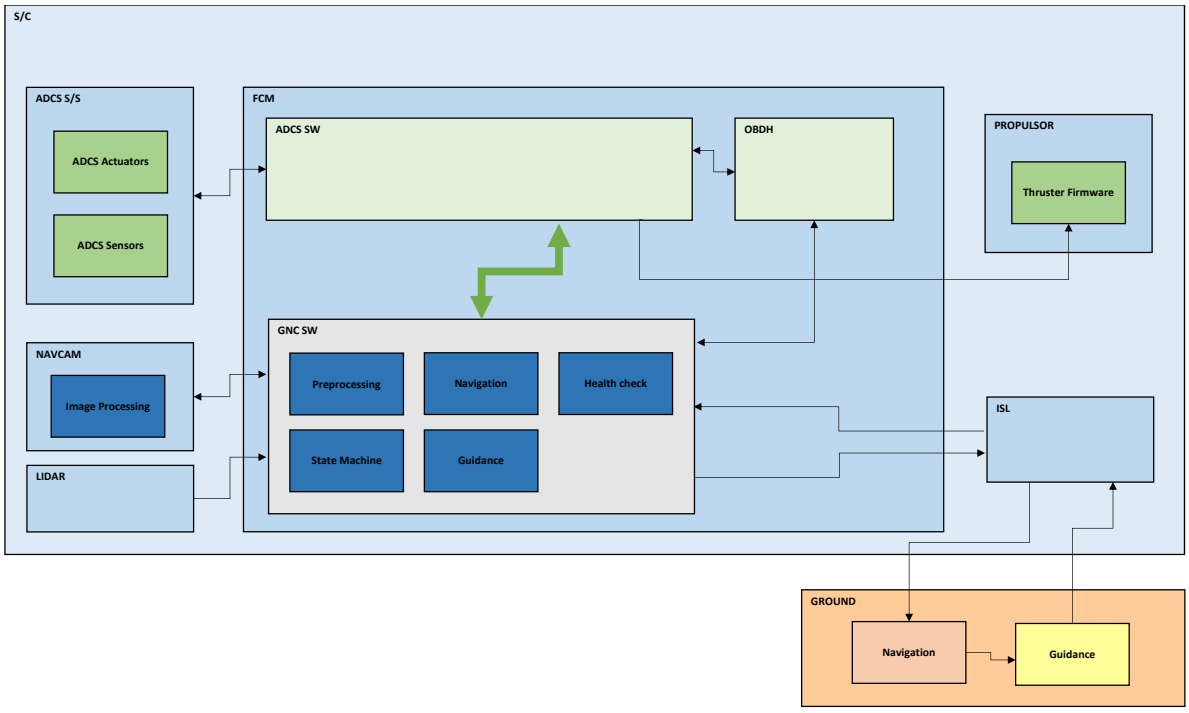

Fig. 5 High-level architecture of the GNC.

The GNC system is being developed in Simulink 2020a* for its simplicity and the capability to convert high-level rapid prototyping code in Matlab/Simulink as C-code via autocoding. This capability would be extremely useful in rapidly converting prototyping code as on-board software code, allowing for a fast iteration between the algorithms design and software code integration in the CubeSat. The key driving requirements for the design of the GNC system have been heavily influenced by the FRP and CRP phases of the mission. On the other end, the concluding portion of the mission, the one of the EXP, has been considered from a design point of view as an experimental phase of the mission. What follows is an overview of the separate elements which constitute the GNC of the Milani CubeSat: the IP, navigation, and guidance and control. Lastly, the autonomous OpNav experiment is briefly explained.

A. IP

The IP and navigation tasks in Milani are deeply interconnected. Milani's on-board navigation strategy relies on optical observables of D1 extracted from images and then used in on-board filters. To do so a robust, simple, and accurate IP method is needed. For the case of Milani, the IP needs to provide reliable data about D1 for navigation, but at the same time to be able to distinguish D2 in the image for pointing purposes. This stems from the consideration that D1 being the largest, most visible, and regular body, would be simpler and more robust to use for navigation. On the other hand, D2 being the focus of the Milani mission is important to be able to distinguish D2 from D1 in the image to eventually be able to point towards it for scientific acquisitions. An object recognition algorithm that distinguishes D1 and D2 based on the areas of the blobs of pixels and an expanding bounding box is put in place to work in the resolved regime of D1, from 4 to 14 km, which is, by design, the applicable range in which FRP and CRP will mostly occur.

Once D1 is distinguished in the image from D2, an IP method is used to extract optical observables to be used for navigation purposes. At the current stage, three methods can be chosen to do so: the COB (Center Of Brightness), WCOB (Weighted COB), and SSWCOB (Sun Sensor WCOB). The first is a special case of the others, which are more sophisticated methods that employ scattering law corrections. All methods are used to extract an estimate of the center of mass of D1 (also called CoF) and the range from D1, which is computed with a simple apparent diameter formula. The difference between the SSWCOB and WCOB lays in the method used to compute the phase angle and the orientation correction of the scattering law. In the WCOB the phase angle is extracted from images while in the SSWCOB is

*https://www.mathworks.com/products/simulink.html, last accessed: 18th November 2021.

extracted from additional data from the Sun sensor. Similarly, for what concern the estimate of the orientation of the correction, in the WCOB it is done by analyzing the image while in the SSWCOB is estimated from the projection of the line of sight of the Sun on the image plane. In general, the SSWCOB is more accurate than the WCOB, but its functioning depends on the availability of Sun sensor data. In this sense, the WCOB is more robust, because it only uses images for its estimate, but proves to be less accurate.

The main characteristic of the WCOB and SSWCOB methods is to correct the Center of Brightness of the body detected in the image with a scattering law. Instead of using an analytical scattering law [19, 20], a data-driven one is employed. This is done so that the IP is capable to work with an irregular-shaped body like the one of an asteroid as D1. To derive the coefficients of the fitting functions used in the WCOB and SSWCOB methods, a global dataset of 10000 images representative of any possible geometric configuration achievable during the Milani mission profile is designed. This is used as a sort of training set to determine which coefficients produce the best fitting functions for the formula illustrated in Equation 1, which is the one of the WCOB:

$$\begin{bmatrix} CoF_x \\ CoF_y \end{bmatrix} = \begin{bmatrix} CoB_x \\ CoB_y \end{bmatrix} + w \times M(PA(e), MajAxisLength) \times \begin{bmatrix} cos(\Phi(eCoB, CoB)) \\ sin(\Phi(eCoB, CoB)) \end{bmatrix} \tag{1}$$

where CoF is the estimated center of the body in the image, CoB is the center of brightness, w is a weighting parameter, M,Φ, and PA are 1D and 2D functions whose coefficients are fit through a training data set, e and $MajAxisLength$ are the eccentricity and major axis length of the blob of pixel labeled as D1, and $eCoB$ is the CoB of the edge region in the asteroid. At the current stage, the data-driven scattering law is applied by exploiting fitting coefficients retrieved from synthetic images of the global dataset. The same approach could be done with real images as well, as for the case of Milani they could be abundantly available from Hera and Dart missions before release. A similar formula as the one in Equation 1 can be used in the SSWCOB with two major differences: the phase angle and the orientation of the correction are not computed using the $PA(e)$ and $\Phi(eCoB, CoB)$ functions, respectively. Instead, they are computed using the line of sight of the Sun in the camera frame. Regardless of the algorithm chosen, a set of optical observables is generated and used in the on-board filter to retrieve a state estimate and relative uncertainties. The WCOB and its variant have been selected after a trade-off with other similar centroiding methods for the specific needs of the Milani mission. In Figure 6 it is possible to see the nominal performance in the CoF estimate of the WCOB method compared with other techniques considered in the trade-off analysis for the FRP and CRP (Center of Brightness, Convex Hull Center of Brightness, Lambertian Sphere Correlation, and WCOB). In Figure 7 it is possible to appreciate the higher accuracy of the WCOB in the CoF estimate. A detailed description of the WCOB is out of the scope of this work. The interested reader is referred to [17, 18] for a more in-depth discussion about the IP of Milani.

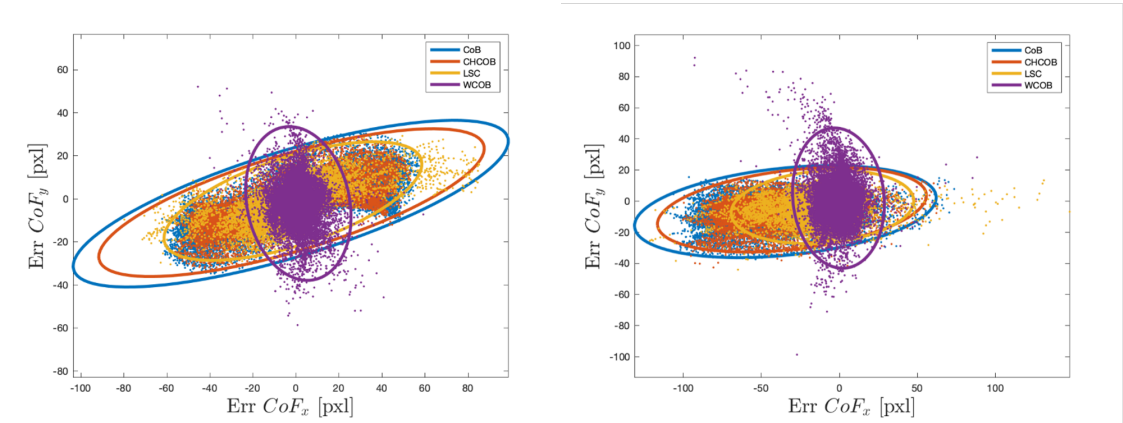

Fig. 6 Error ellipses of the CoF estimates in the FRP (left) and CRP (right) phases of the Milani mission in the image plane of the Milani NavCam for different algorithms tested.

B. Navigation

The nominal navigation strategy of the Milani mission is based on images, lidar, and radio-tracking data collected over the mission duration and processed on ground. However, a parallel on-board navigation strategy is designed for

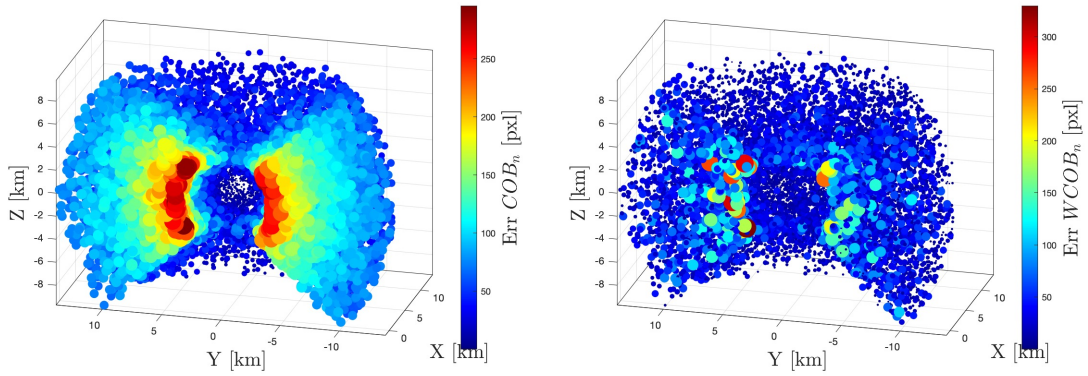

Fig. 7 Magnitude of the CoF error of the COB (left) and WCOB (right) in the global dataset of images representative of all geometric conditions seen during the mission timeline.

pointing purposes and as part of a technology demonstration experiment. This strategy uses the optical observables collected by the IP together with lidar data to estimate the relative state of the CubeSat with respect to D1. In doing so it is important to note that optical observables are assumed not to be available below 4 km (by design this is the nominal distance at which D1 saturates the NavCam's FOV) and that lidar data is assumed not to be available above 5.5 km as a consequence of the expected albedo of D1. The set of observables available to the on-board filter will thus vary with the range from D1. Also note that even though below 4 km optical observables are considered too degraded to be used in the filter, they can still be used to provide rough information for pointing.

The choice of the on-board navigation filter has been based on the performances of EKF (Extended Kalman Filter) and UKF (Unscented Kalman Filter) variants. The UKF gives slightly better performance, given the non-linear dynamical environment, but it requires a significantly higher computational effort. Therefore, the choice has been made to use an EKF for the on-board application. The current on-board navigation strategy assumes to employ optical observables every 1800 s and lidar data every 300 s, given the slow dynamics that characterize Milani's trajectories. If the filter is called without any new measurement, it only performs a forward propagation of the state. Process noise is introduced to account for residual accelerations and the uncertainty related to the SRP perturbation. Thus, two Gauss-Markov (GM) processes are considered, whose characteristics are given in Table 1.

Table 1 Gauss–Markov processes properties

	σ	τ
Residual acceleration	$5 \times 10^{-9} m/s^2$	1 day
Solar Radiation Pressure	8% of SRP acceleration	1 day

Finally, range and range-rate information between Hera and Milani that can be exchanged via ISL are not used for navigation purposes for two main reasons. First, to be useful for on-board navigation with respect to the system they would need to be accompanied in near real-time by the ephemerides of the Hera spacecraft, which would add complexity from an operational point of view. Second, even with Hera ephemerides continuously transmitted on-board, these would be affected by navigation errors on the Hera's state that could make them potentially unreliable for navigation of Milani. For these reasons, ISL data is not used in the current navigation strategy on-board Milani.

C. Guidance and Control

After the navigation solution is provided, in the proposed GNC architecture of Milani the translational guidance and control follow a robust ground-based approach. Even Collision Avoidance Maneuvers (CAMs) are designed to be computed on ground. Supported by sensor data from Milani and by the Orbit Determination (OD) of the spacecraft around the system, the collision risk assessment (with respect to Hera, Juventas, D1, and D2) as well the maneuver computation and execution is entirely relegated on ground. This simplifies the on-board architecture and avoids

introducing elements of risk in terms of execution of false-positive CAMs.

On the other hand, the most important output of the GNC system of Milani is the generation of a primary attitude profile for the ADCS. To provide this quantity, three main pointing strategies are designed:

- **Reference**: It is the simplest one and consists in providing a pointing profile without the need of having sensors or ADCS readings. The pointing profile is computed easily from geometric considerations using the ephemerides of the bodies of the system, which are stored on-board. In this strategy, also the ephemerides of Milani need to be communicated from ground, which may not be conservative in case of off-nominal scenarios and could in general introduce higher pointing errors.
- **Tracking**: The attitude estimated by the ADCS and the output of the IP are exploited to track the target and keep it at the center of the NavCam FOV. The main parameter of this strategy is the tracking time, the interval between images used to update the primary pointing.
- **Predicted**: It uses the estimated trajectory with the on-board filter together with ephemerides of the desired target (D1, D2, Hera, Juventas, or ad hoc-selected feature on the body such as the crater region) to compute the desired pointing. This pointing mode is particularly relevant when D2 is not recognized as a different body than D1 by the IP. In those cases, the need to perform scientific acquisitions is guaranteed by the on-board filter's solution without intervention from ground.

With these strategies in place, and with the support of the IP, the ADCS, and the rest of the GNC system, Milani shall be capable to provide a reliable primary pointing quaternion to the ADCS for scientific acquisitions and nominal operations, never losing the desired body from the FOV of the camera. Should that occur, a lost in space scenario mode would be adopted. In this mode, the CubeSat would autonomously scan the surrounding environment from the last known appearance of the bodies in the FOV, while ensuring specific geometric constraints on the sun direction are met.

Milani will thus demonstrate the capability to autonomously navigate around the Didymos binary system and employ this capability for a practical pointing purpose throughout the FRP and CRP phases of the mission. In the next session, it is shown how the autonomous IP and navigation capabilities of Milani will be tracked on the ground within the framework of a proposed autonomous optical navigation experiment.

D. Autonomous optical navigation experiment

As described in the previous section, the GNC of Milani will attempt at the best of its capability to generate a state estimate as part of its tasks. This estimate, however, will not be used for the translational guidance and control but will be used to generate a primary pointing for the ADCS. An autonomous navigation experiment is therefore designed based on the collection of more data about the available sensors, IP, and Navigation filter throughout the mission lifetime. The techniques used on-board of Milani can then be replicated on the ground and compared with higher-fidelity ones. This assessment will provide a useful technology demonstration experiment for future missions. A con-ops of the experiment is illustrated in Figure 8.

The Autonomous Optical Navigation (AutOpNav) experiment is an opportunistic technology demonstration experiment whose goal is to test Milani's optical navigation and its capability to support autonomous navigation in the proximity of an asteroid. As mentioned, the experiment is opportunistic and does not interfere with the nominal operations of Milani. The specific goal of the experiment is to test the algorithms for on-board image processing and on-board navigation filtering. The outcome of the on-board algorithms will be validated against on-ground techniques. If successful, the AutOpNav experiment would be a crucial step towards enabling the on-board implementation of the translational guidance and control of a CubeSat for an asteroid mission.

The experiment is de-facto based on a data-collection strategy executed during all operational phases of the mission (FRP, CRP, and EXP). The set of data to be transmitted and elaborated on-ground is made of low-level sensor data such as ranges from the lidar and images from the NavCam, but also by high-level processed data such as IP observables and filter's output. A crucial part of the experiment is to allow for this set of 4 telemetry data to be transmitted asynchronously on-ground as part of the nominal telemetry of the GNC system. The frequency at which each set is transmitted is opportunistic and largely depends on its packet size. IP, filter, and lidar data are expected to be abundantly available and of low size for transmission. On the other hand, images are expected to be the heaviest set to be transmitted. For this reason, the first is going to be activated more frequently than required during nominal operations, while the latter is going to exploit the already planned captures for the ground-based orbit determination process.

On the ground, the data is used to demonstrate the on-board performance of the IP and filter. To validate filter performance, the ground-based OD solution of the Milani trajectory is used as a reference. To achieve this goal, the IP data related to images downlinked for on-ground OD are also considered and included in the telemetry stream. This

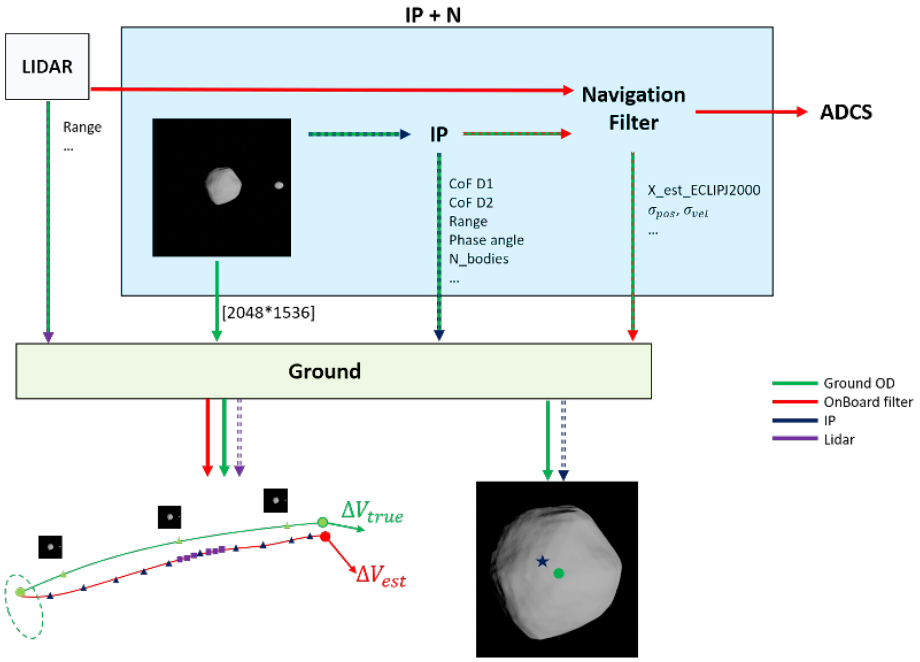

Fig. 8 Con-ops of the autonomous navigation experiment.

enables a direct comparison between the on-board IP algorithms and the on-ground more refined ones, given that they will be applied to the same input. Since no additional images are downlinked to ground other than those needed for orbit determination, the data budget of the mission is not stressed by this experiment.

The con-ops in Figure 8 illustrates the AutOpNav experiment, with signals flowing asynchronously in the IP and navigation blocks toward the ADCS and Ground. The red lines represent the connections that support nominal ADCS operations. The green lines represent signals downlinked to ground for the nominal ground-based OD process, to reconstruct Milani trajectory. The purple, blue and red links represent additional data that is downlinked to perform the experiment and assess the on-board capability of the IP and filter. The experiment is designed to be run as close as possible to real-time, as a sort of shadow-engineering simulation which is also useful to monitor closely the performance of the GNC system. An additional element for this experiment could be the simultaneous usage of the TinyV3RSE facility [21] to reproduce the optical environment in the Didymos system. With such a facility, it would be possible to test the robustness of the IP in a higher fidelity environment. The facility, the experiment, and the on-board software replica would thus not only be passively used to provide an independent orbit determination solution with the raw data and processing capabilities that would be available on-board, but could be deployed actively as a design analog, to change and tune the GNC parameters during flight operations to increase the performances and ensure stability.

IV. Results

In this section, some results achieved by the GNC system described in the previous sections are illustrated. For simplicity, only the performance of the GNC over arcs 1 and 2 of the FRP and CRP phases are illustrated, for a total of 4 cases. These are considered to be representative of the performance of all arcs of these two phases of the mission. The IP has been set to generate optical observables with the WCOB method every 1800 s above 4 km while lidar data is collected every 300 s below 5.5 km. The same set of figures is obtained for each case. For simplicity, the IP performance is presented first, followed up by the navigation performance.

In Figure 9, Figure 11, Figure 13, and Figure 15 the estimated CoM (the CoF) of D1 is compared with its true projection in the Milani NavCam as function of time. In Figure 10, Figure 12, Figure 14, and Figure 16 the other output of the IP, the estimated range and phase angle, are also visualized with their true values.

Finally, the performance of the on-board navigation filter are illustrated in Figure 17, Figure 18, Figure 19, and Figure 20. The filter error is reported in camera frame with the 3σ bounds for all components.

In Figure 21 some global metrics for the 4 cases of the IP and navigation are compared together.

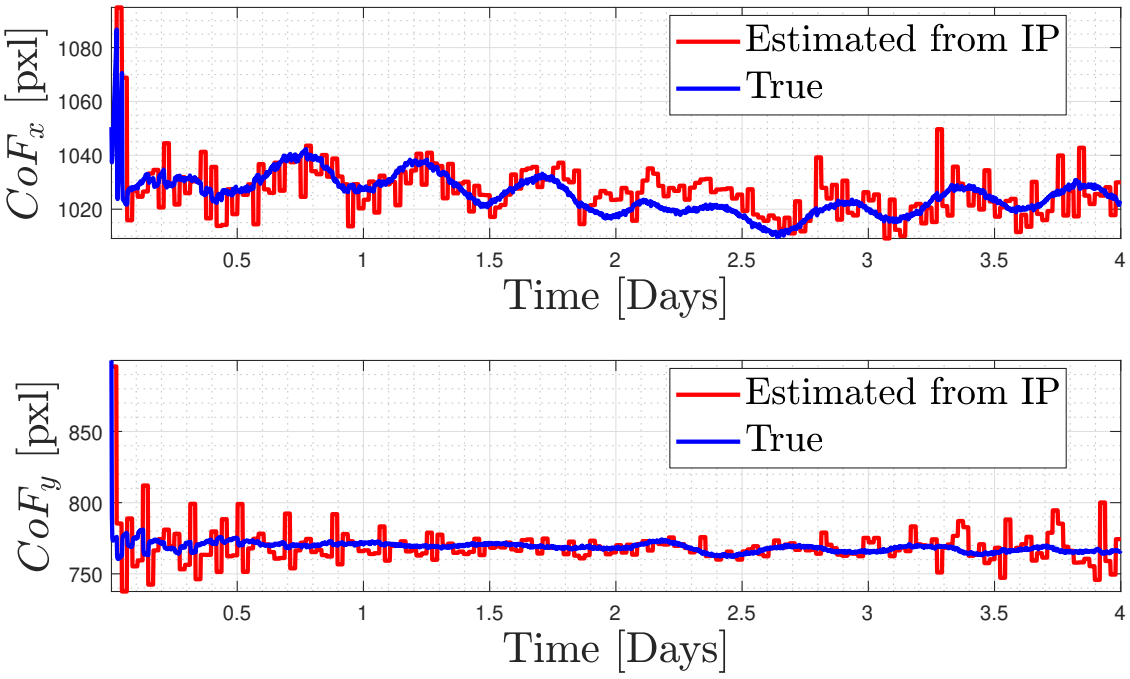

Fig. 9 Performance of the CoF estimate of the WCOB method in FRP arc 1.

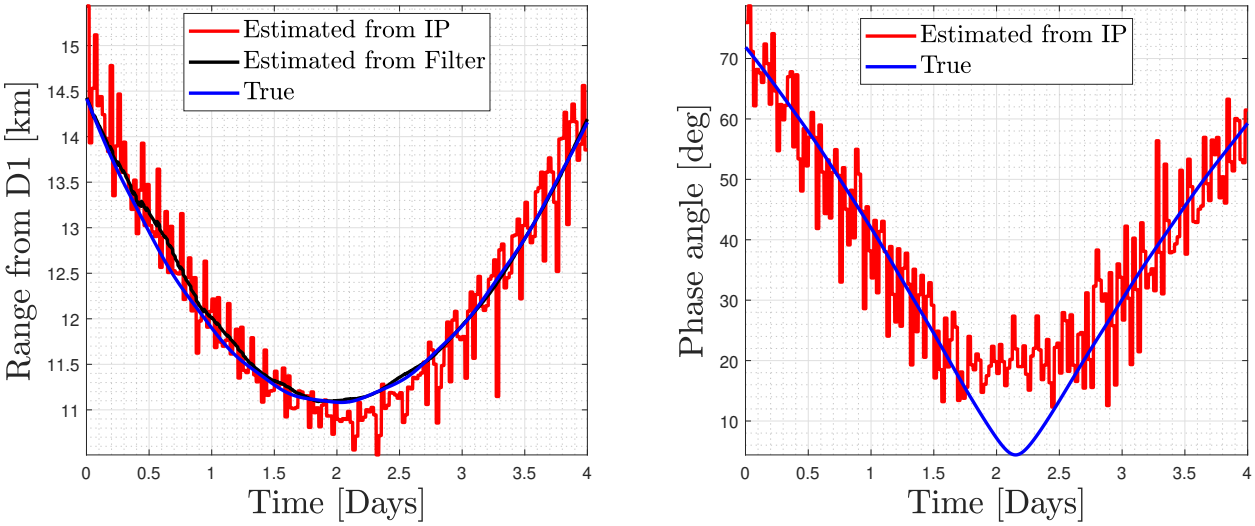

Fig. 10 Performance of the range and phase angle estimates of the WCOB method in FRP arc 1.

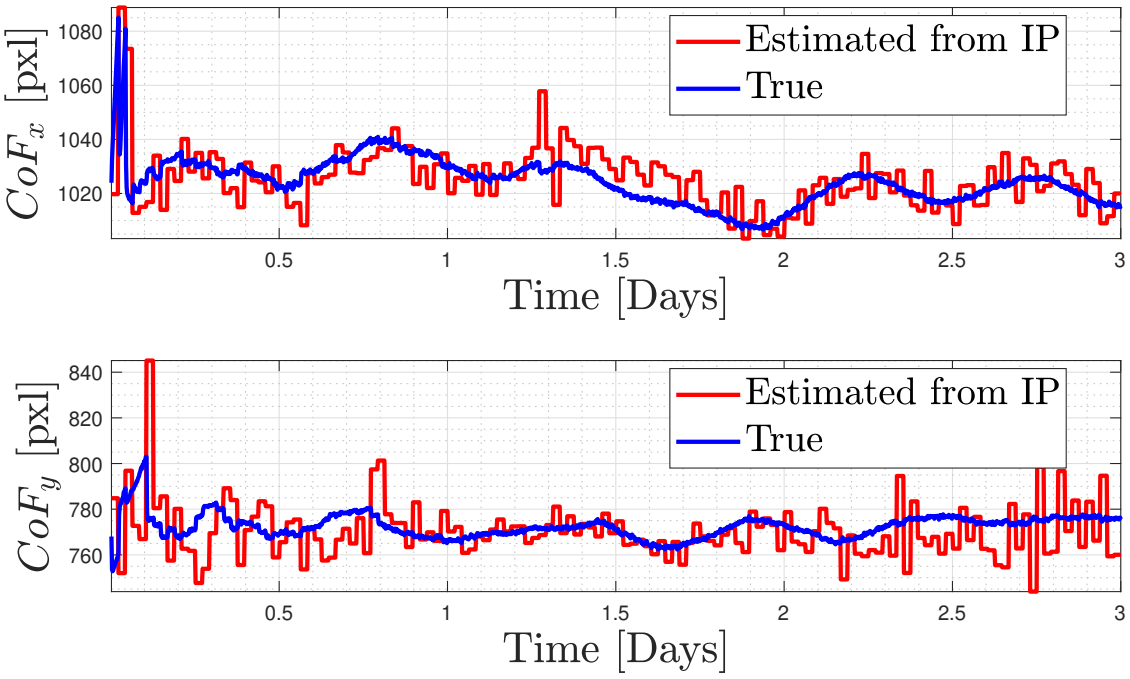

Fig. 11 Performance of the CoF estimate of the WCOB method in FRP arc 2.

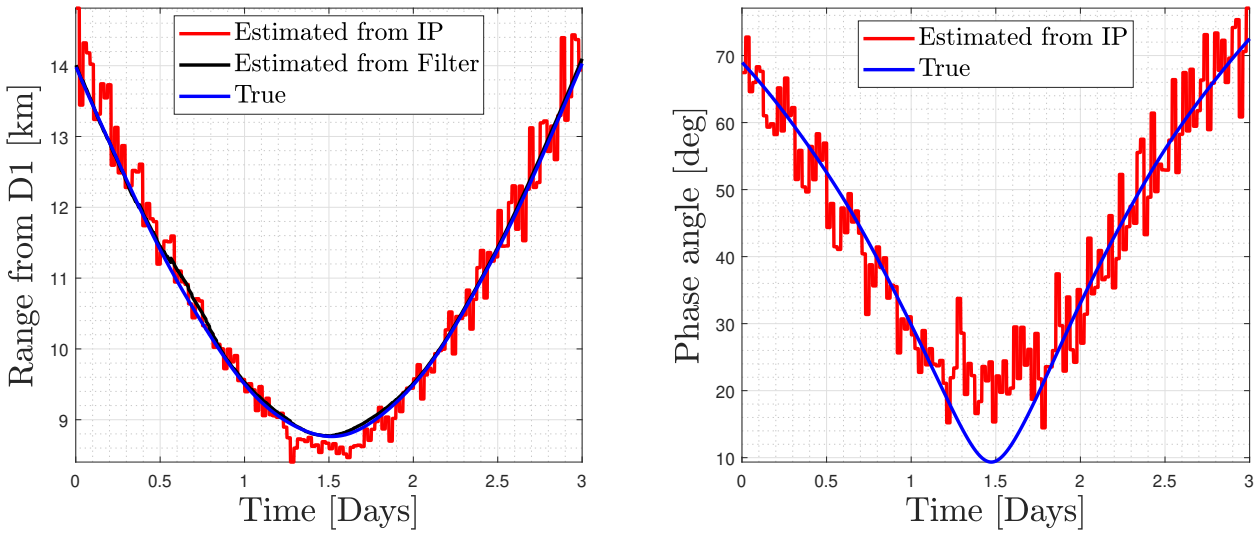

Fig. 12 Performance of the range and phase angle estimates of the WCOB method in FRP arc 2.

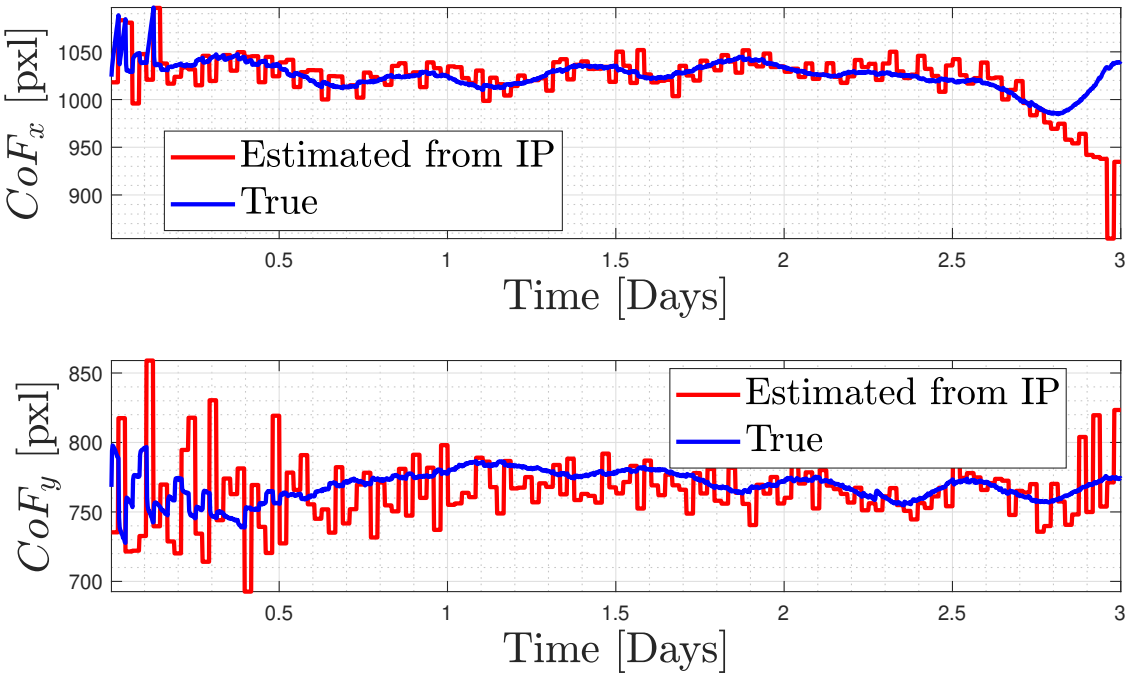

Fig. 13 Performance of the CoF estimate of the WCOB method in CRP arc 1.

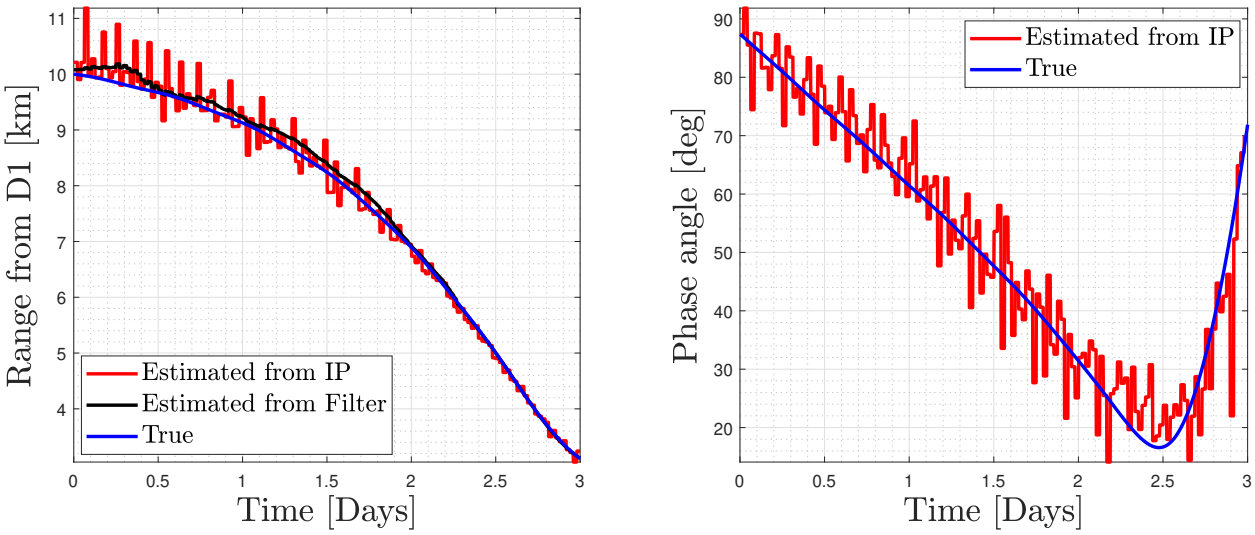

Fig. 14 Performance of the range and phase angle estimates of the WCOB method in CRP arc 1.

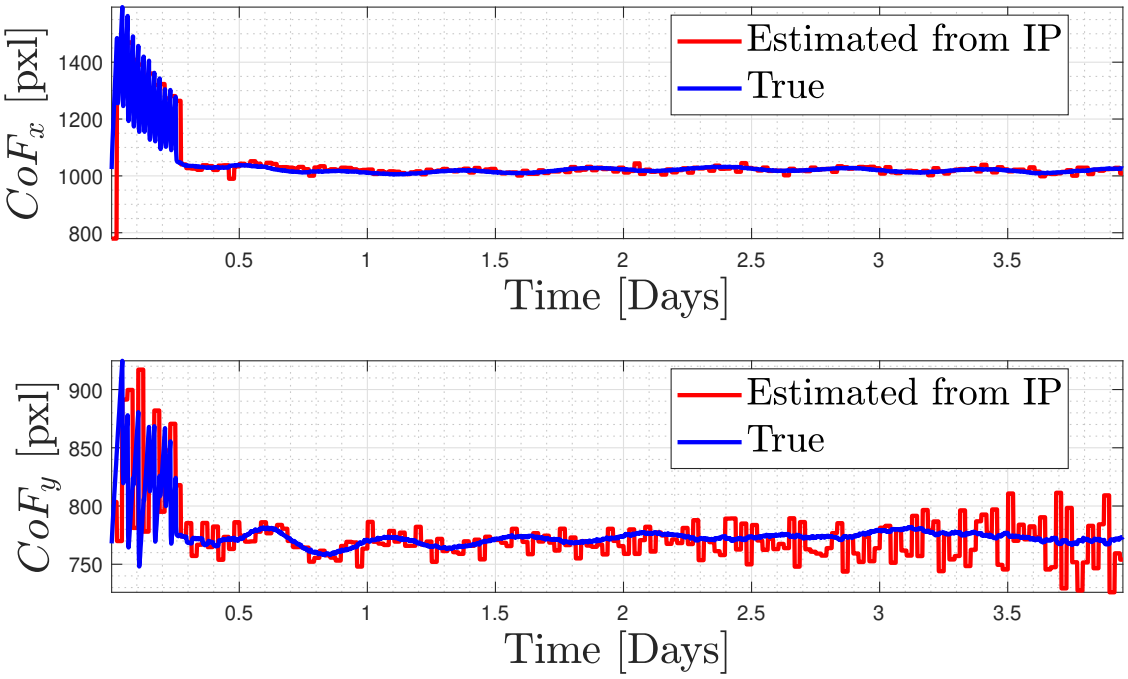

Fig. 15 Performance of the CoF estimate of the WCOB method in CRP arc 2.

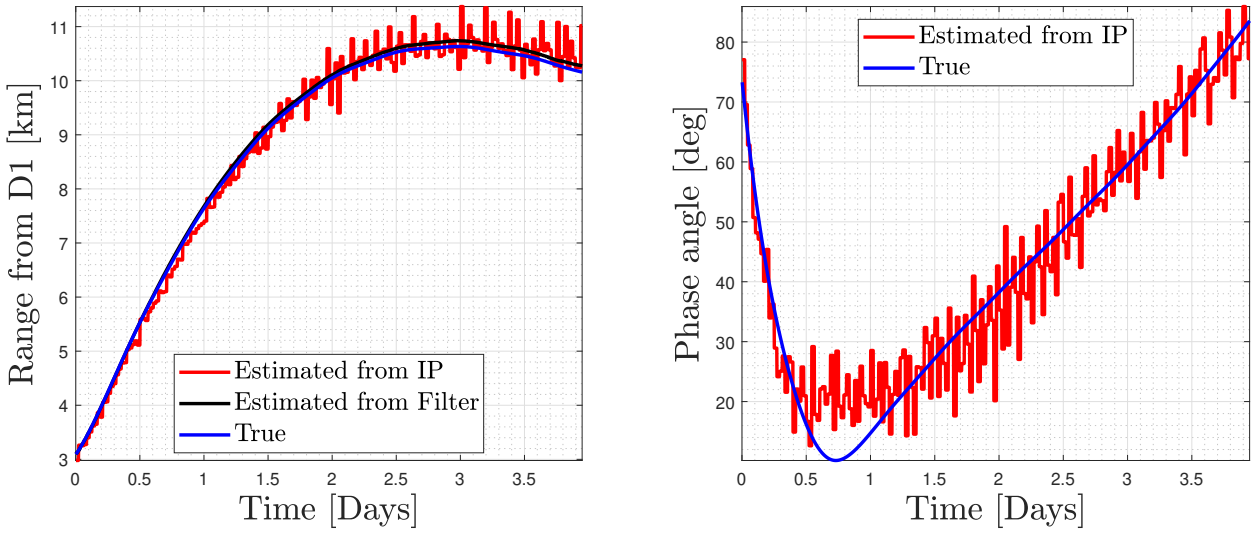

Fig. 16 Performance of the range and phase angle estimates of the WCOB method in CRP arc 2.

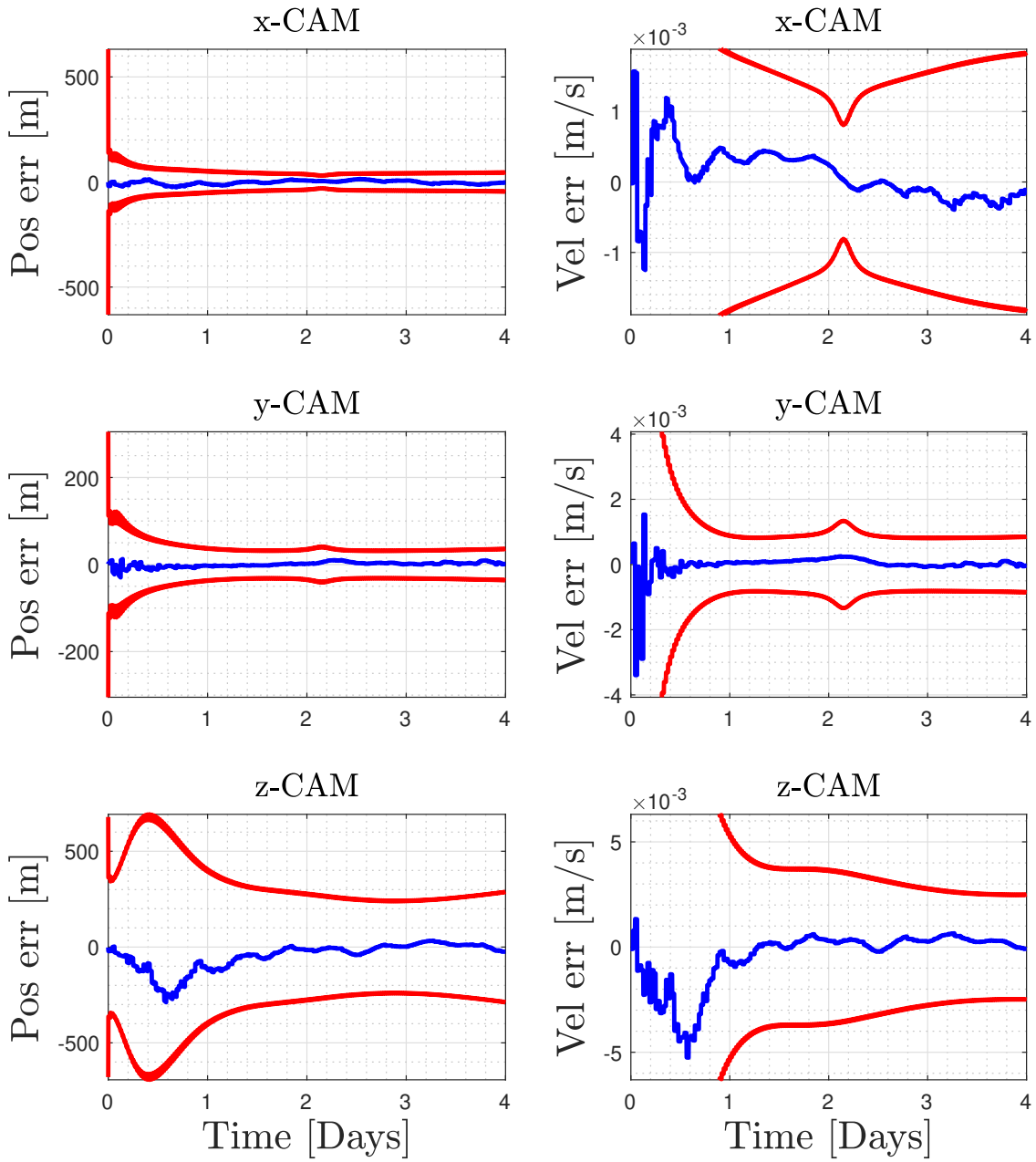

Fig. 17 Performance of the filter in FRP arc 1 with the axes in camera frame.

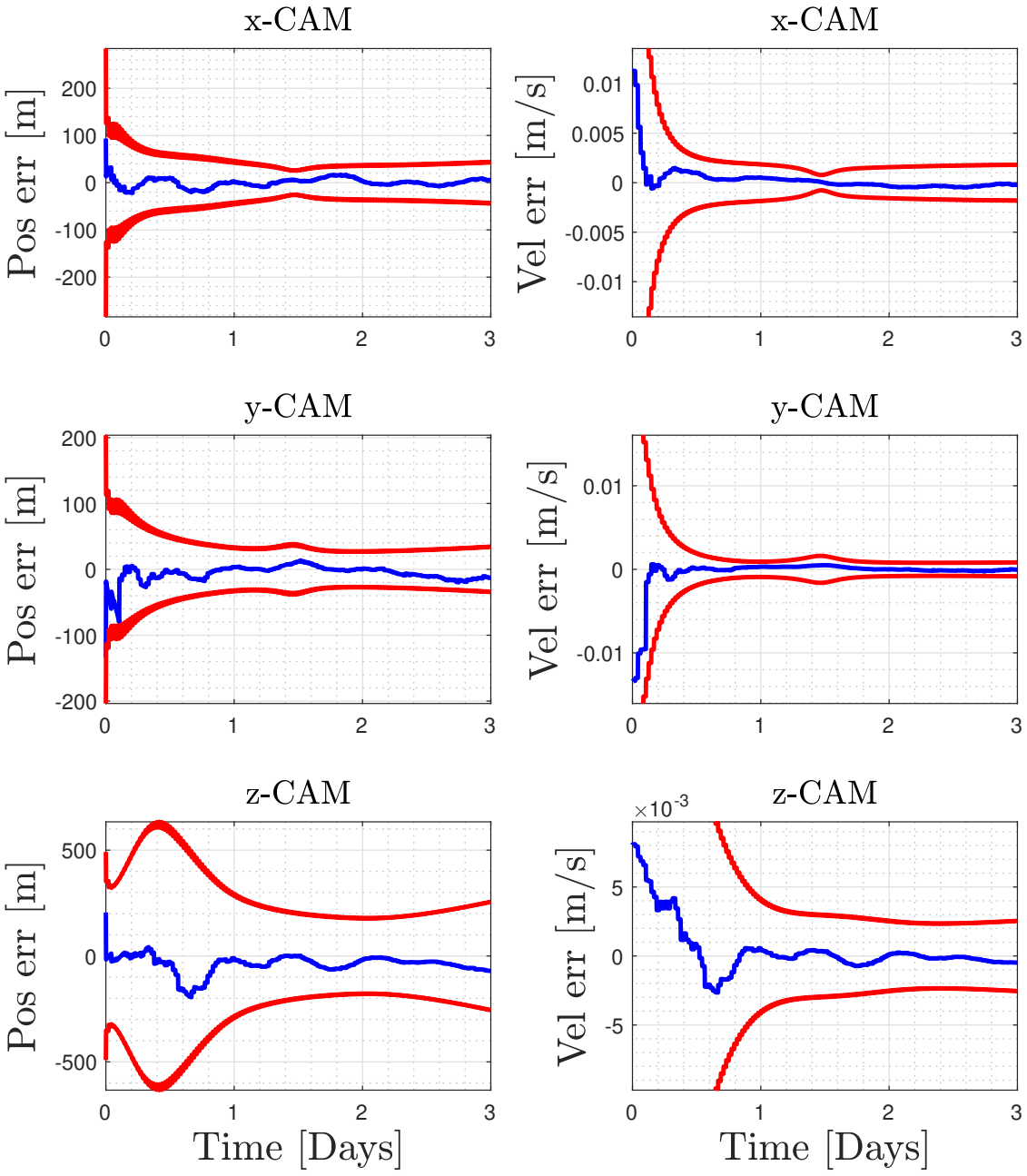

Fig. 18 Performance of the filter in FRP arc 2 with the axes in camera frame.

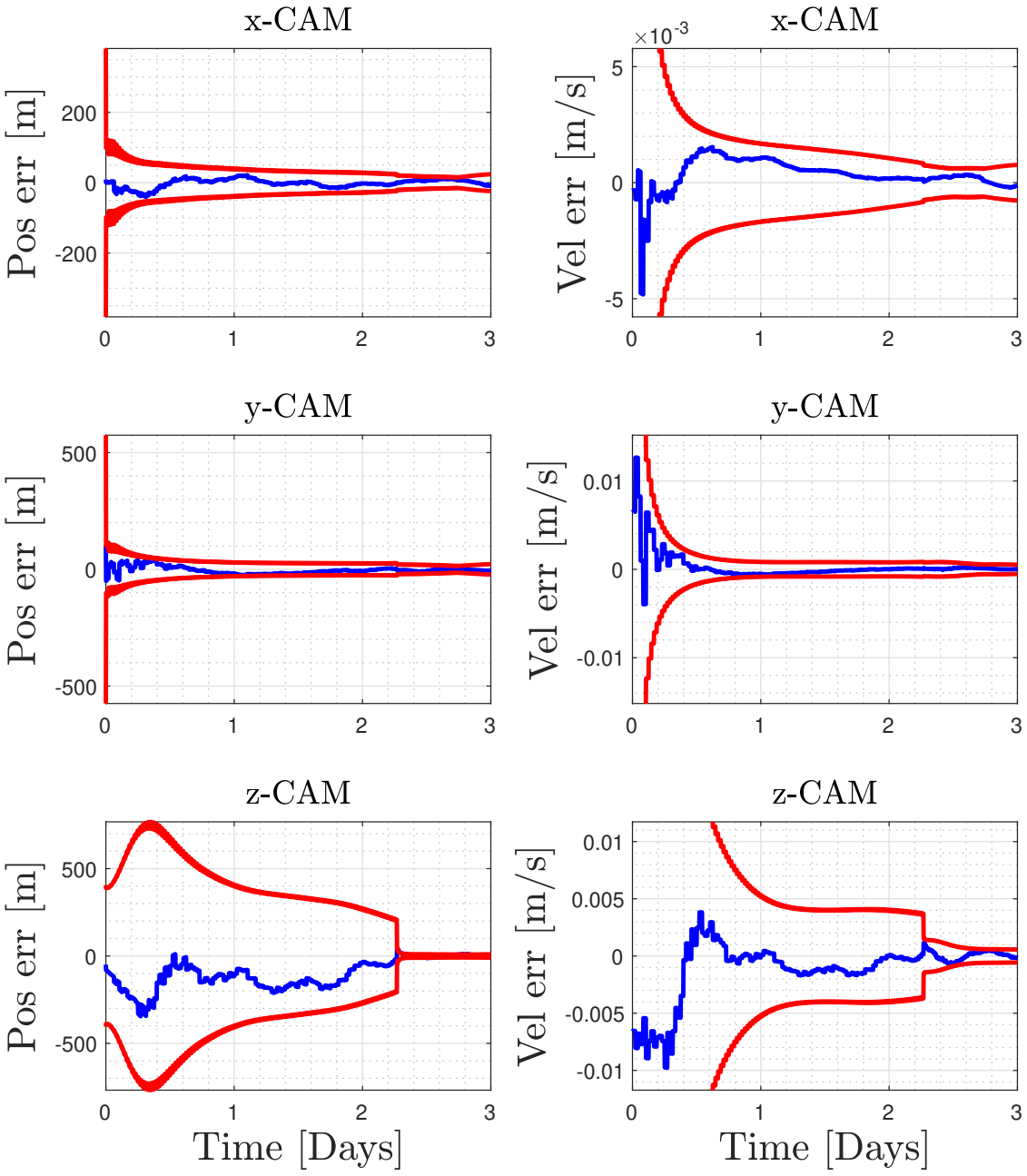

Fig. 19 Performance of the filter in CRP arc 1 with the axes in camera frame.

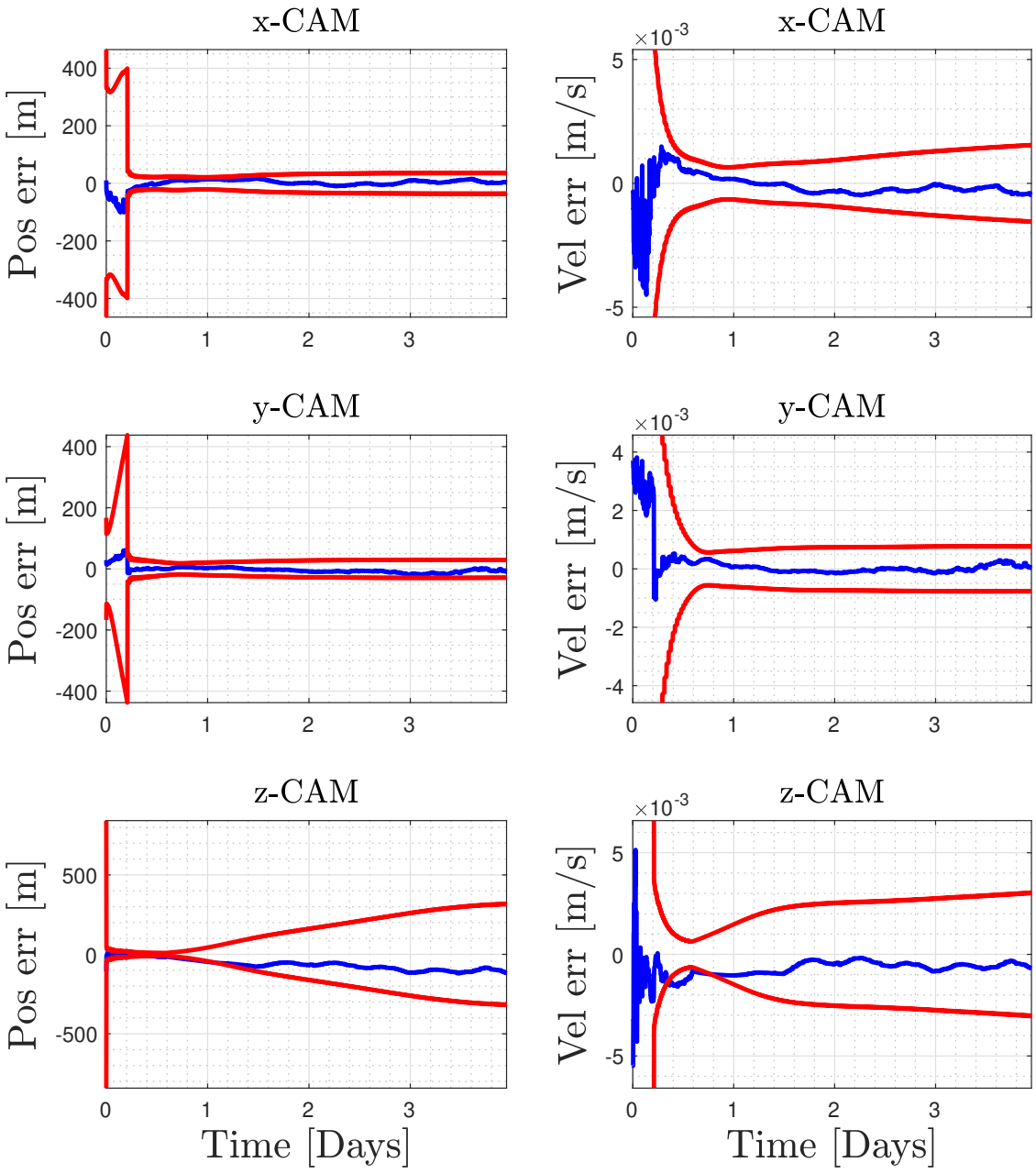

Fig. 20 Performance of the filter in CRP arc 2 with the axes in camera frame.

From the analysis of the performance of the IP in the FRP arcs, it is possible to see that the algorithm performed well. It is possible to observe in both arcs of the FRP that the IP consistently overestimated the phase angle at low values (see Figure 10 and Figure 12.). This in turn reflects into the poor performances of the WCOB in determining the correct CoF_x coordinate in this interval, as it is possible to see in Figure 9 and Figure 11. For what concerns the CRP arcs, similar conclusions can be drawn, but illustrated on asymmetrical arcs. What is interesting to note for the CRP cases is the behavior of the WCOB method at the end of arc 1 and at the beginning of arc 2, in Figure 13 and Figure 15, respectively. It is possible to see large deviations between the real and estimated CoF, in both components. This is because the algorithm is now applied below 4 km and outside its design region. Note that the observations from the WCOB are not used in the filter for this reason.

For what concern the navigation performance, it is possible to see that in all cases but one (CRP arc 2, the z component of the velocity in camera frame) the estimated state stays well within the 3σ values and convergence of the filter is achieved within few days after initialization. In the CRP cases (at the end of CRP arc 1 and the beginning of CRP arc 2) the beneficial effect of the lidar on the navigation solution is noticeable, especially in the boresight direction.

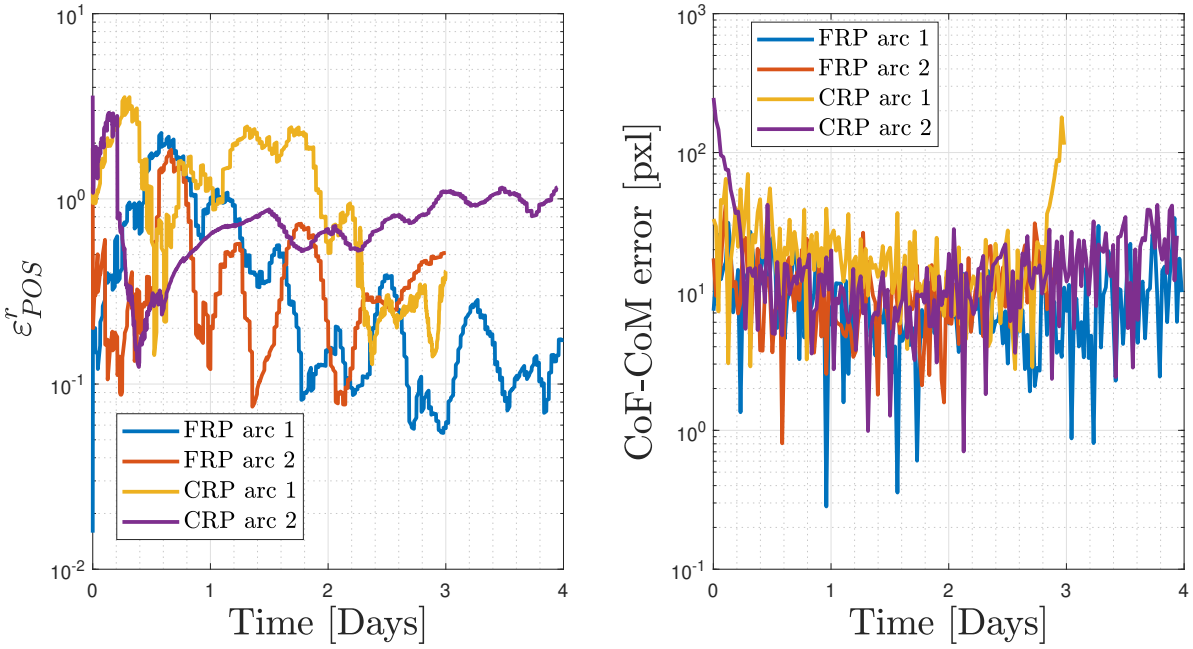

Fig. 21 Relative percentage on-board positioning error for all arcs (left), and WCOB error on all arcs (right).

Finally, from Figure 21 it is possible to have a view on the global IP and navigation performance of the GNC system of Milani. In particular, from the analysis of the 4 cases presented in this work, we can conclude that the relative positioning error (with respect to the true range) always stays below 4 % for all cases. Similarly, the IP method and the WCOB algorithm seem to perform well for the entire duration of the arcs considered (excluding the performance below 4 km, outside of the design range). The algorithm achieves a mean error in the CoF estimate of roughly 10 pixel for the FRP arcs and 20 pixel for the CRP arcs.

V. Conclusions

In this work a generic overview of the Milani mission is provided together with a detailed description of its GNC system. Preliminary results in some representative and geometrically challenging arcs of the FRP and CRP phases are illustrated, showing good IP and navigation performances. Milani design is currently in phase C and is fast approaching a CDR in spring 2022. The main challenges for the immediate future is the implementation of the algorithms and strategies described in this work with a robust architectures for an on-board software implementation. Morevoer, future work will be focused on further validation and verification campaigns to test the robustness and performances of the GNC.

Acknowledgments

This work is part of the ESA contract No. 4000131925/20/NL/GLC for the mission phases A/B/C/D/E of Milani. The authors would like to acknowledge the support received by the whole Milani consortium, which is lead by Tyvak International. M.P and F.T would like to acknowledge the funding received from the European Union's Horizon 2020 research and innovation programme under the Marie Skłodowska-Curie grant agreement No 813644.

References

[1] Glassmeier, K.-H., Boehnhardt, H., Koschny, D., Kührt, E., and Richter, I., "The Rosetta mission: flying towards the origin of the solar system," *Space Science Reviews*, Vol. 128, No. 1, 2007, pp. 1–21. DOI: 10.1007/s11214-006-9140-8.

[2] Yoshikawa, M., Kawaguchi, J., Fujiwara, A., and Tsuchiyama, A., "Hayabusa sample return mission," *Asteroids IV*, Vol. 1, 2015, pp. 397–418. DOI: 10.2458/azu_uapress_9780816532131-ch021.

[3] Watanabe, S. i., Tsuda, Y., Yoshikawa, M., Tanaka, S., Saiki, T., and Nakazawa, S., "Hayabusa2 mission overview," *Space Science Reviews*, Vol. 208, No. 1, 2017, pp. 3–16. DOI: 10.1007/s11214-017-0377-1.

[4] Lauretta, D., Balram-Knutson, S., Beshore, E., Boynton, W., d'Aubigny, C. D., DellaGiustina, D., Enos, H., Golish, D., Hergenrother, C., Howell, E., et al., "OSIRIS-REx: sample return from asteroid (101955) Bennu," *Space Science Reviews*, Vol. 212, No. 1, 2017, pp. 925–984. DOI: 10.1007/s11214-017-0405-1.

[5] Snodgrass, C., and Jones, G. H., "The European Space Agency's comet interceptor lies in wait," *Nature communications*, Vol. 10, No. 1, 2019, pp. 1–4. DOI: 10.1038/s41467-019-13470-1.

[6] Michel, P., Küppers, M., and Carnelli, I., "The Hera mission: European component of the ESA-NASA AIDA mission to a binary asteroid," *COSPAR Scientific Assembly*, Pasadena, California, 2018, pp. 1–42.

[7] Walker, R., Binns, D., Bramanti, C., et al., "Deep-space CubeSats: thinking inside the box," *Astronomy & Geophysics*, Vol. 59, No. 5, 2018, pp. 5–24. DOI: 10.1093/astrogeo/aty237.

[8] Michel, P., Cheng, A., and Küppers, M., "Asteroid Impact and Deflection Assessment (AIDA) mission: science investigation of a binary system and mitigation test," *European Planetary Science Congress*, Vol. 10, 2015, pp. 123–124.

[9] Atchison, J. A., Ozimek, M. T., Kantsiper, B. L., and Cheng, A. F., "Trajectory options for the DART mission," *Acta Astronautica*, Vol. 123, 2016, pp. 330–339. DOI: 10.1016/j.actaastro.2016.03.032.

[10] Dotto, E., Della Corte, V., Amoroso, M., Bertini, I., Brucato, J., Capannolo, A., Cotugno, B., Cremonese, G., Di Tana, V., Gai, I., et al., "LICIACube-the Light Italian Cubesat for Imaging of Asteroids in support of the NASA DART mission towards asteroid (65803) Didymos," *Planetary and Space Science*, 2021, p. 105185. DOI: 10.1016/j.pss.2021.105185.

[11] Goldberg, H., Karatekin, O., Ritter, B., et al., "The Juventas CubeSat in Support of ESA's Hera Mission to the Asteroid Didymos," *Small Satellite Conference*, 2019, pp. 1–7.

[12] Ferrari, F., Franzese, V., Pugliatti, M., Giordano, C., and Topputo, F., "Preliminary mission profile of Hera's Milani CubeSat," *Advances in Space Research*, Vol. 67, No. 6, 2021, pp. 2010–2029. DOI: 10.1016/j.asr.2020.12.034.

[13] Ferrari, F., Franzese, V., Pugliatti, M., Giordano, C., and Topputo, F., "Trajectory Options for Hera's Milani CubeSat Around (65803) Didymos," *The Journal of Astronautical Sciences*, 2021. DOI: 10.1007/s40295-021-00282-z.

[14] Bottiglieri, C., Piccolo, F., Rizza, A., Giordano, C., Pugliatti, M., Franzese, V., Ferrari, F., and Topputo, F., "Trajectory design and orbit determination of Hera's Milani CubeSat," *2021 AAS/AIAA Astrodynamics Specialist Conference*, 2021, pp. 1–15.

[15] Kohout, T., Cardi, M., Näsilä, A., Palomba, E., Topputo, F., and the Milani team, "Milani CubeSat for ESA Hera mission," *European Planetary Science Congress 2021*, 13–24 Sep 2021. DOI: 10.5194/epsc2021-732.

[16] Dirri, F., Palomba, E., Longobardo, A., Biondi, D., Boccaccini, A., Galiano, A., Zampetti, E., Saggin, B., Scaccabarozzi, D., and Martin-Torres, J., "VISTA Instrument: A PCM-Based Sensor for Organics and Volatiles Characterization by Using Thermogravimetric Technique," *2018 5th IEEE International Workshop on Metrology for AeroSpace (MetroAeroSpace)*, IEEE, 2018. DOI: 10.1109/metroaerospace.2018.8453532.

[17] Pugliatti, M., Franzese, V., and Topputo, F., "Data-driven Image Processing for Onboard Optical Navigation Around a Binary Asteroid," *Journal of Spacecraft and Rockets*, 2021. In press.

[18] Pugliatti, M., Franzese, V., Piccolo, F., Rizza, A., Bottiglieri, C., Giordano, C., Ferrari, F., and Topputo, F., "Design of the on-board image processing of the Milani mission," *2022 AAS GN&C conference*, 2022. Accepted.

[19] Bhaskaran, S., Riedel, J. E., and Synnott, S. P., "Autonomous nucleus tracking for comet/asteroid encounters: the Stardust example," *1998 IEEE Aerospace Conference Proceedings*, Vol. 2, 1998, pp. 353–365.

[20] Liounis, A. J., "Limb Based Optical Navigation for Irregular Bodies," , 2018. 1st Annual RPI Workshop on Image-Based Modeling and Navigation for Space Applications, Troy, NY.

[21] Pugliatti, M., Franzese, V., Panicucci, P., and Topputo, F., "TinyV3RSE: The DART vision-based navigation test bench," *32nd AIAA/AAS Space Flight Mechanics Meeting*, 2022.